Al-doped Yttrium Iron Garnets $Y_3AlFe_4O_{12}$: Synthesis and Properties

A. Belous, A. Tovstolytkin, O. Fedorchuk, Yu. Shlapa, S. Solopan, B. Khomenko

PII: S0925-8388(20)34503-5

DOI: https://doi.org/10.1016/j.jallcom.2020.158140

Reference: JALCOM158140

To appear in: *Journal of Alloys and Compounds*

Received date: 10 July 2020
Revised date: 24 November 2020
Accepted date: 26 November 2020

Please cite this article as: A. Belous, A. Tovstolytkin, O. Fedorchuk, Yu. Shlapa, S. Solopan and B. Khomenko, Al-doped Yttrium Iron Garnets $Y_3AlFe_4O_{12}$: Synthesis and Properties, *Journal of Alloys and Compounds,* (2020) doi:https://doi.org/10.1016/j.jallcom.2020.158140

Al-doped Yttrium Iron Garnets $Y_3AlFe_4O_{12}$: Synthesis and Properties

A. Belous[1], A. Tovstolytkin[2], O. Fedorchuk[1], Yu. Shlapa[1], S. Solopan[1], B. Khomenko[1]

[1]V. I. Vernadskii Institute of General and Inorganic Chemistry of the NAS of Ukraine, 32/34 Palladina avenue, Kyiv 03142, Ukraine

[2]Institute of Magnetism of the NAS of Ukraine and MES of Ukraine, 36-b Vernadskogo Blvd., Kyiv 03142, Ukraine

A method to synthesize nanosize particles of $Y_3AlFe_4O_{12}$ garnet ferrite by precipitation in aqueous solutions at constant pH during the synthesis has been demonstrated. The effect of the sequence of the metal hydroxides precipitation on the filtration coefficient is studied. The filtration coefficient is found to be three times greater in the case of simultaneous precipitation of iron and aluminum hydroxides compared to the one observed for the case of simultaneous precipitation of all hydroxides. Synthesized precipitates are established to be amorphous and crystalline nanoparticles are formed in one stage after the treatment at 800 °C. The average particles size is around 60 – 70 nm. The ceramics obtained after a proper heat treatment of the nanoparticles is shown to be characterized by the high density and good electrophysical properties.

Keywords: yttrium iron garnet, consecutive precipitation, crystalline structure, particle morphology, magnetization, ferromagnetic resonance.

Background

$R_3Fe_5O_{12}$ ferrites with garnet structure were discovered in the 50th years of the 20th century. Since then, these materials have received great attention in science and technology owing to extraordinary properties such as high electrical resistance, low magnetic losses beyond the region of the ferromagnetic resonance (FMR) (damping constant is approx. 10^{-5} [1]), relatively high saturation magnetization,

narrow FMR line (~ 0.2 Oe in single crystals), high thermal and chemical stability, low thermal expansion, and others. Due to these advantages, $R_3Fe_5O_{12}$ ferrites have found a number of applications in magnetooptical filters [2], magnetooptical recording devices [3-6], microwave and magnonic elements [7-10], multifunctional elements in communication, electronic and spintronic devices [11, 12], and in the systems of 5G wireless technology [13].

Electrophysical properties of polycrystalline garnet ferrites depend on a number of factors, such as a method of synthesis, size of crystallites, purity of chemicals, etc. Yttrium iron garnet (YIG) is the most typical representative among the ferrite garnets. YIG has the cubic structure and crystalizes in the *Ia-3d* space group. Cations in YIG are located in the three sublattices (dodecahedral (24), octahedral (16) and tetrahedral (24)). Such structure can be described by a general formula of $\{R_3\}[Fe_2](Fe_3)O_{12}$, where {}, [] and () brackets indicate the positions in the dodecahedral, octahedral and tetrahedral sublattices, respectively. As a rule, Y^{3+} occupies the dodecahedral positions, and Fe^{3+} ions occupy tetrahedral and octahedral positions in the ratio of 2:3. Yttrium ions are non-magnetic and, thus, magnetic properties are caused by the presence of the iron ions in the tetrahedral and octahedral sublattices.

In an ideal case, the magnetic moments of Fe^{3+} ions in different sublattices are antiparallel, but in some cases, the iron ions of the tetrahedral sublattice can leave their positions and occupy the positions in the dodecahedral sublattice. In this case, the yttrium ions have to occupy the free nodes in the tetrahedral lattice. Therefore, the spontaneous magnetization of the material is dependent on the cation distribution between different crystalline sites. The values of the saturation magnetization and magnetic anisotropy for a typical YIG are $4\pi M_s$ = 1750 G and H_a = 40 Oe, respectively [14].

An introduction of dopants or change of the synthesis method can be employed for the purposeful governing of the properties of YIG. Partial substitutions are applicable for all cation sublattices. In a number of recent works,

the substitutions of yttrium ions by the ions of the rare-earth elements (La, Nd, Ce, Eu, Yb, Ho, Pr, …) [13, [15] - [19]] or bismuth ions [[20]] have been considered. Also the substitutions of iron ions by the ions of Zn, Ni, Co, Cu have been studied [[21], [22]].

Many scientists perform simultaneous doping in two cation sublattices, for instance, by the ions of bismuth and manganese ($Y_{3-x}Bi_xFe_{5-x}Mn_xO_{12}$) [[23]] or ions of calcium and tin ($Y_{3-x}Ca_xFe_{5-x}Sn_xO_{12}$) [[24]]. It allows obtaining the magnetic parameters, which are necessary for certain microwave devices.

Recently, the garnet ferrites, where iron is partially substituted by aluminum, have attracted an enhanced attention of researchers and technologists [[25]-[29]]. Such polycrystalline ferrites are characterized by the low dielectric and magnetic losses, their coercive force decreases and dielectric constant slightly grows [27]. At the same time, it is known that there are significant differences in the properties of yttrium iron-aluminum garnets (YIAG), which have the same composition but synthesized via different methods [25, 27, 28]. Therefore, it is important to develop the controlled preparation method to obtain the desired distribution of cations, desired crystal structure and phase formation since the synthesis and post-synthesis process (sintering) techniques have a profound effect on the properties of garnets on the nanoscale.

There are many well-known methods for the synthesis of the garnet ferrites, such as solid-state synthesis, sol-gel method (Pechini method) [[30]], precipitation in the aqueous solutions, hydrothermal synthesis [[31]], precipitation in microemulsions and many others [[32]]. Each of the methods has its own advantages and drawbacks. In particular, the solid-state method does not provide a sufficient level of homogeneity of the product and does not allow obtaining small size particles that results in the necessity to use high temperatures (>1500 °C) for the synthesis of the ceramic samples. Sol-gel method requires the application of the expensive alkoxides and does not allow synthesizing a large amount of the material. Similar drawbacks are typical for other methods of synthesis, including precipitation in the

microemulsions [27, [33]]. Moreover, it is practically impossible to wash out the reaction side products after the sol-gel synthesis.

At the same time, the precipitation in the aqueous solutions is relatively cheap method that allows obtaining a large amount of the nanoparticles. However, this kind of the synthesis method is usually performed using the sodium hydroxide solution as the precipitator, which results in the pollution of the precipitates by the sodium ions. Therefore, the obtained products need the long-term washing to completely remove the sodium ions, since they have negative impact on the electrophysical properties of the materials in the microwave range. Moreover, such precipitates are amorphous and are poorly filtered and washed out that does not permit the complete removing of the sodium ions. For this reason, a search for better ways to improve the filtration mode and washing out such precipitates is very important.

Therefore, the aim of this study is (1) to develop a method of the synthesis of Al-doped solid-solutions of $Y_3AlFe_4O_{12}$ garnet ferrites by the precipitation in the aqueous solutions, which would give the possibility to obtain the weakly-agglomerated nanoparticles with good ability to be washed out from the sodium ions; (2) to look for a way to reduce the temperature of obtaining the ceramic materials below 1500 °C, and (3) to study the effect of the synthesis conditions on the physical parameters of the powders and ceramic samples based on the obtained nanoparticles.

2. Materials and Methods

2.1. Synthesis of $Y_3AlFe_4O_{12}$ powders

The method of the precipitation in aqueous solutions has some technological nuances, which require the particular attention. For example, it is important to preliminary determine and precisely maintain a ratio of the concentrations of starting reagents for obtaining a target chemical composition. In this work, based

on our earlier experience, the aqueous solutions of $Y(NO_3)_3$, $Fe(NO_3)_3$ and $Al(NO_3)_3$ in concentrations of each salt 1.5 mol/l were used as the starting reagents for the synthesis of $Y_3AlFe_4O_{12}$ nanoparticles via precipitation in aqueous solutions.

To investigate the reproducibility of the results, each sample was synthesized twice. In each case, around 100 g of the final powder was produced.

Aqueous solutions of sodium hydroxide NaOH or ammonium hydroxide NH_4OH in the concentrations of 10 mol/l were used as the precipitator. Precipitation of metal hydroxides during the synthesis of $Y_3AlFe_4O_{12}$ ferrite was performed by several approaches:

1) Stoichiometric amounts of metal salts were precipitated simultaneously using NaOH solution at the constant pH of the medium 8.8 ÷ 8.9 (*Sample 1*).

2) Consecutive precipitation using the solution of NaOH: the precipitation of $Fe(OH)_3$ at pH 4 ÷ 4.5 was followed by that of the mixture of $Al(OH)_3$ and $Y(OH)_3$ at pH 8.8 ÷ 8.9 (*Sample 2*).

3) Consecutive precipitation using the solution of NaOH: the precipitation of the mixture of $Fe(OH)_3$ and $Al(OH)_3$ hydroxides at pH 4 ÷ 4.5 was followed by that of the $Y(OH)_3$ hydroxide at pH 8.8 ÷ 8.9 (*Sample 3*).

4) Consecutive precipitation using the solution of NH_4OH: the precipitation of the mixture of $Fe(OH)_3$ and $Al(OH)_3$ hydroxides at pH 4 ÷ 4.5 was followed by that of the $Y(OH)_3$ hydroxide at pH 8.8 ÷ 8.9 (*Sample 4*).

Precipitation of 100 g of the final product of each sample was performed for 4 hours at the intensive stirring, the solutions of salts were dropped with the rate of 5 – 10 ml/min. Obtained suspensions were heated up to the 80 °C and held at this temperature for 1 hour to achieve the solutions aging [34]. Filtration of the suspensions and washing out the precipitates were performed by the hot (70-80°C)

bidistilled water in the proportion of 200 l/kg. The time of washing was estimated for each sample individually.

Atomic-absorption spectroscopy was used to determine the concentration of sodium ions in the filtrate after washing out the precipitate of hydroxide powders with different amount of water (100 l/kg, 150 l/kg and 200 l/kg).

Filtration coefficient of the precipitates was calculated by Darcy formula:

$$Q = K_f S \frac{H}{l} \tau \quad (1)$$

where Q is the volume of the filter, cm^3; K_f – the filtration coefficient, cm/s; S – the area of the precipitate on the filter, cm^2; H – the rarefaction under the filter, cm. water col.; l – the thickness of the precipitate layer, cm; τ - time of the filtration, s [35].

2.2. Synthesis of the ceramic samples based on $Y_3AlFe_4O_{12}$ powders

The preliminary synthesized $Y_3AlFe_4O_{12}$ powders subjected to the heat treatment at 800 °C for 2 hours in the air were used for the preparation of the ceramic samples. The products obtained after heat treatment were milled with water in the ball-mill with metallic balls for 4 hours. 15%-solution of the binding component and 3% of aqueous solution of polyvinyl alcohol were added to the powder and corresponding tablets were pressed under the pressure of 2 ton/cm^2. The prepared tablets were dried at 70-90 °C, warmed up in the muffle furnace with the heating rate of 5 °C/min to 1350 °C and kept at 1350-1400 °C for 2 hours.

2.3. Study of the properties of the ferrite samples.

Differential thermal analysis (DTA) of the synthesized hydroxide powders of ferrite precursors was carried out using the derivatograph Q-1000 up to the 1000 °C.

X-ray analysis (XRD) of the powders and ceramic samples was performed using the diffractometer DRON-4 (Cu$K\alpha$ – radiation). The level of crystallinity was determined according to the method described in [36] using the software *Origin Pro* 9.0.

Electron microscopic studies of the synthesized powders were performed using the transmission electron microscope (TEM) *JEM* 1400 (Jeol, Japan).

Microstructural investigations of the polished surfaces of the ceramic samples were performed using the scanning electron microscope SEC miniSEM SNE 4500MB (SEC Co., Ltd, South Korea)

Magnetic measurements were carried out at room temperature with the use of an LDJ-9500 vibration sample magnetometer.

Dielectric constant of the ceramics was measured using the *Agilent N5230A PNA–L Network Analyzer* and a specific cell for measurements, which included the 3-section X-band waveguide with the cross-sectional area of 23×10 mm^2 and two metallic diaphragms [37, 38]. Investigated samples were placed into the rectangular waveguide between the centers of the wide walls of the waveguide. The samples were in the shape of rectangular parallelepipeds with the average cross-sectional area of 1.1×1.1 mm^2 and the length of 10 mm. The error of the measurements, which may originate from the inaccuracy in the sample geometry, is about 10 %.

The samples in the form of thin discs with the sizes of H = 0.7 mm and D = 3 mm were used for the determination of the width of the ferromagnetic resonance (FMR) line. The installation for the measurements consisted of the spectrometer PE1306, magnetic induction meters SH-1 and SH-8, frequency meter CHZ-39, frequency transformer YA34-19, electromagnet and system for binding the samples with the rotated cylinder and computer with necessary software [39, 40]. Each sample was fixed in the cylinder binding between the poles of the electromagnet that made it possible to change the position of a sample relatively to

the magnetic field. Obtained FMR spectra were used to determine the width of the FMR line. The error in the determination of the FMR linewidth did not exceed ± 0.2 Oe.

3. Results and Discussions

The filtration coefficients for all synthesized powders were calculated to estimate the filtration rate of the precipitates from the sodium ions. The results obtained are summarized in Table 1. The highest filtration coefficient was found to be for the *Sample 3*, while the lowest one – for the *Sample 4*. The reason for the latter feature can originate from the strong agglomeration of the particles due to the formation of the amorphous gels of aluminum hydroxide using the ammonium solution as the precipitator [41].

Table 1. Filtration coefficient of the hydroxide precursor powders and concentration of the sodium ions in the filtrate

No of the sample	Filtration coefficient (cm/s)	Concentration of Na^+ after washing of 100 l/kg H_2O mg/l	Concentration of Na^+ after washing of 150 l/kg H_2O mg/l	Concentration of Na^+ after washing of 200 l/kg H_2O mg/l
1	2.2×10^{-7}	0.39	<0.20	<0.00
2	5.5×10^{-7}	0.33	0.20	<0.00
3	6.5×10^{-7}	0.23	0.02	<0.00
4	$1,2\times10^{-7}$	Absent	Absent	Absent

Table 1 lists the values of the concentration of the sodium ions in the filtrate after washing out the hydroxide powders for *Samples 1-3* with the different volume of water (100 l/kg, 150 l/kg, 200 l/kg) estimated by the atomic-adsorption spectroscopy.

Sample 4 was free of the sodium ions since it precipitated by the ammonium solution during the synthesis.

Representative results of the differential-thermal analysis for the synthesized precursor of ferrite powders are shown in Fig. 1. The presence of two endothermic effects in the temperature ranges of 100-200 °C and 300-400 °C is observed for all synthesized samples. The first endothermic effect on the DTA curves corresponds to the loss of the sorption water in nanoparticles, and the second one – to the loss of the crystallization water [42]. The principal mass reduction due to the loss of the sorption and crystallization water occurs up to 500 °C and equals approx. 77%.

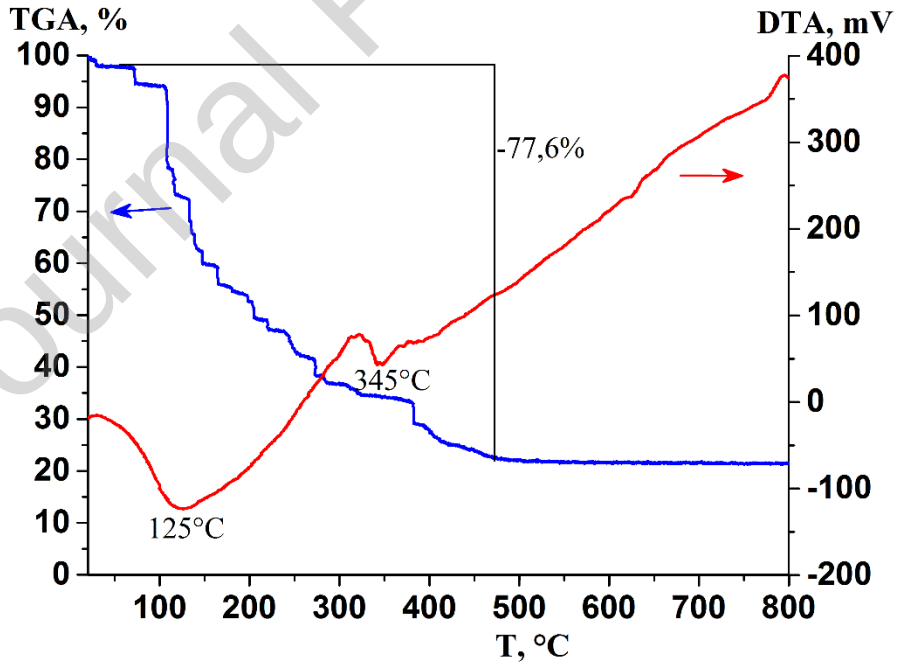

Fig. 1. Representative DTA curves of the ferrite powder for *Sample 3*

The features of the formation of the crystalline garnet structure were investigated by the X-ray diffraction method. X-ray patterns for the samples heat treated in the temperature range of 300 – 800°C are shown in Fig. 2. The presence

of the amorphous halo at 2θ = 25-40° on the patterns points to the fact that the particles synthesized at temperatures lower than 700 °C are amorphous. At the same time, the crystalline garnet structure is formed in one-stage just after the heat treatment at 800 °C without formation of any intermediate phases.

According to the results of XRD studies, *Samples 3* and *4* synthesized after the heat treatment at 800 °C are single-phase, but the traces of the additional Fe_2O_3 phase are observed to be present in *Samples 1* and *2* (Fig. 3).

Taking into account these results, the temperature for the synthesis of the samples was chosen to be 800 °C that allowed us to achieve high "chemical activity" of the powder and, at the same time, to keep the temperature of the synthesis as low as possible.

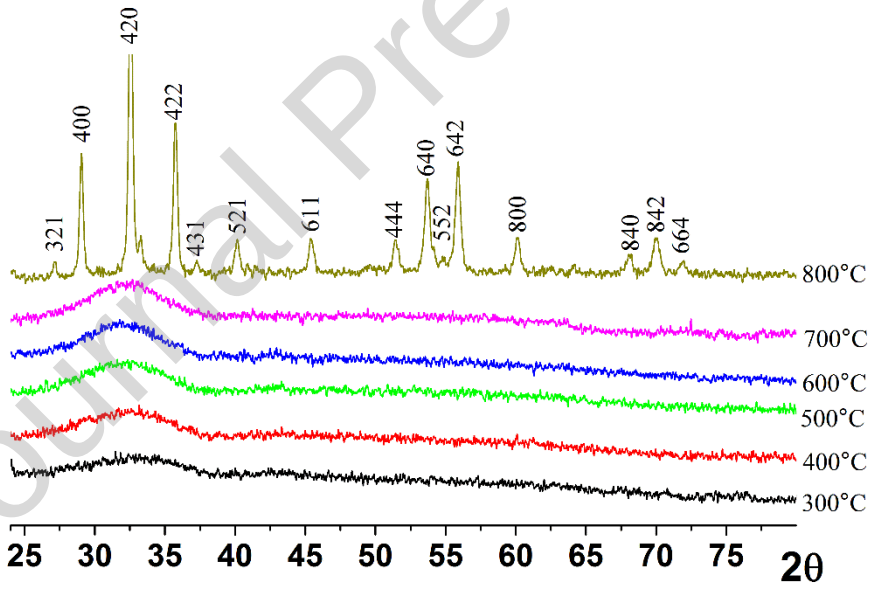

Fig. 2. XRD patterns for $Y_3AlFe_4O_{12}$ ferrite (*Sample 3*) after the heat treatment at 300 – 800°C for 2 hours.

The analysis of the obtained patterns shows that the crystalline structure for all synthesized YIAG nanopowders is cubic with the space group of *Ia-3d* in the correspondence with the patterns database (JCPDS No 43- 0507). Calculated crystallographic parameters of the particles are summarized in Table 2.

Determination of the average size of the particles was done via a Sherrer method using corresponding XRD patterns, and the level of crystallinity for the particles was calculated as described in [36].

The calculations performed showed that all synthesized ferrite nanoparticles after the heat treatment at 800 °C had the average sizes of 60-70 nm and their level of crystallinity was in the range of 51-78 %. It was established that the change of the crystallographic parameters of the synthesized samples is a function of the method of synthesis and it is in good correlation with the calculated particles sizes and their level of crystallinity. The increase of the cell parameters of nanoparticles can originate from their structural defectiveness, which depends on the individual factors for each sample. For example, it may be caused by a low level of crystallinity for *Sample 2* and by a small average size of the particles for *Sample 4*.

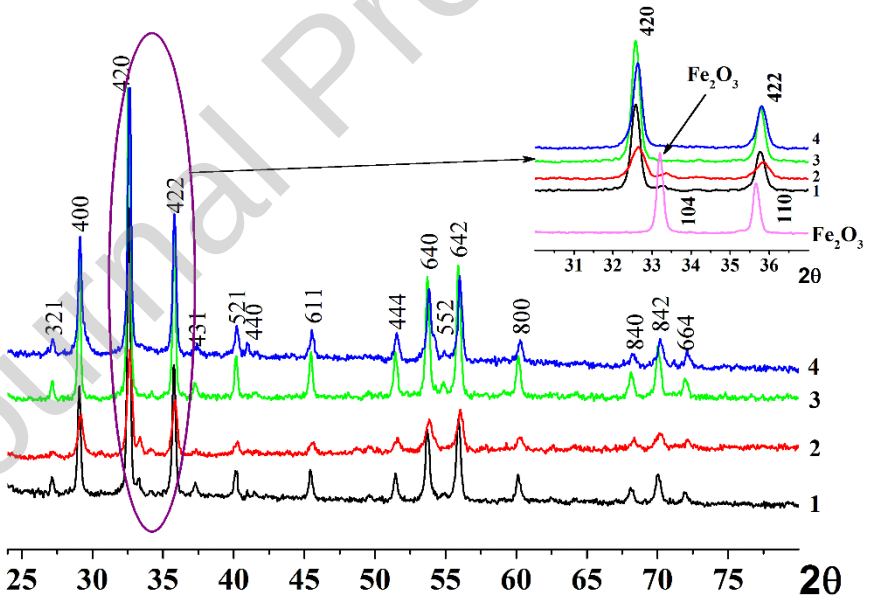

Fig. 3. XRD patterns for the ferrite nanoparticles after the heat treatment at 800 °C for 2 hours: 1 – *Sample 1*; 2 – *Sample 2*; 3 – *Sample 3*; 4 – *Sample 4*. The enlarged region with the peaks of α-Fe_2O_3 is shown in the inset.

Table 2. Crystallographic parameters and average particle sizes for the $Y_3AlFe_4O_{12}$ ferrite nanoparticles

	a (Å)	*V* (Å^3)	R_f*	R_{Bragg}**	Level of crystallinity (%)	$D_{X\text{-}Ray}$ (nm)
Sample 1	12.322(3)	1871.1(8)	7.3	8.7	78	59
Sample 2	12.340(1)	1879.0(3)	3.38	4.96	51	67
Sample 3	12.324(2)	1872.0(7)	6.4	7.6	72	65
Sample 4	12.366(1)	1891.3(2)	6.8	7.3	72	59

*R_f is compliance form factor; **R_{Bragg} is Bragg factor

Electron microscopy investigations (TEM) were performed to study the morphology of $Y_3AlFe_4O_{12}$ ferrite nanoparticles, and a representative TEM-image is shown in Fig. 4. The sizes of the particles were calculated using the obtained data. The average sizes of the particles are found to be in the range of 50-70 nm and these data are in good agreement with those estimated from XRD results. It should be noted that the strong agglomeration is observed for the nanoparticles, which can originate from a relatively high temperature of their treatment (800 °C).

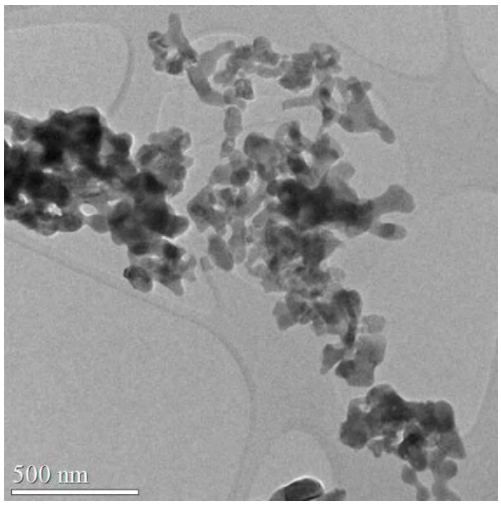

Fig. 4. TEM image of the ferrite nanoparticles (*Sample 3*) after the heat treatment at 800 °C.

The field dependences of the magnetization for the YIAG nanoparticles heat-treated at 800 °C are shown in Fig. 5a. The main magnetic parameters of the nanoparticles are summarized in Table 3. As it can be observed, *Samples 1* and *3* are characterized by the highest values of the saturation magnetization and the lowest values of the coercive force. It means that the formation of the garnet structure is faster in *Samples 1* and *3*, compared to *Samples 2* and *4*.

To analyze magnetic properties of pure and substituted YIG, one should keep in mind that among the five iron ions, which are included in a formula unit $Y_3Fe_5O_{12}$, two are in octahedral sites and three are in tetrahedral sites. A magnetic moment of 5 μ_B per formula unit results from antiferromagnetic superexchange interaction between Fe^{3+} ions in these two different sites through the intervening O^{2-} ions (here, μ_B is Bohr magneton) [43].

In substituted YIG, the smaller ion persistently seeks a smaller site [43]. It is known that in garnet-type structures, the tetrahedral site is smaller than the octahedral one. For this reason, in our case, at low levels of substitution, the tetrahedral substitution is preferred by Al ions, but as Al concentration gets increased, after some critical substitution level (around $x \approx 0.7$) Al ions display a tendency toward octahedral substitution [44]. As a result, there is a site distribution of Al ions between octahedral and tetrahedral sites. In this case, the correct formula for $Y_3Al_xFe_{5-x}O_{12}$ can be written as $\{Y_3\}[Fe_{2-y}Al_y](Fe_{3-z}Al_z)O_{12}$ ($x = y + z$), where {} denotes the sublattice formed by Y^{3+} ions occupying dodecahedral sites, [] – the sublattice formed by Fe^{3+} and Al^{3+} ions occupying octahedral sites, and () – the sublattice formed by Fe^{3+} and Al^{3+} ions occupying tetrahedral sites [44].

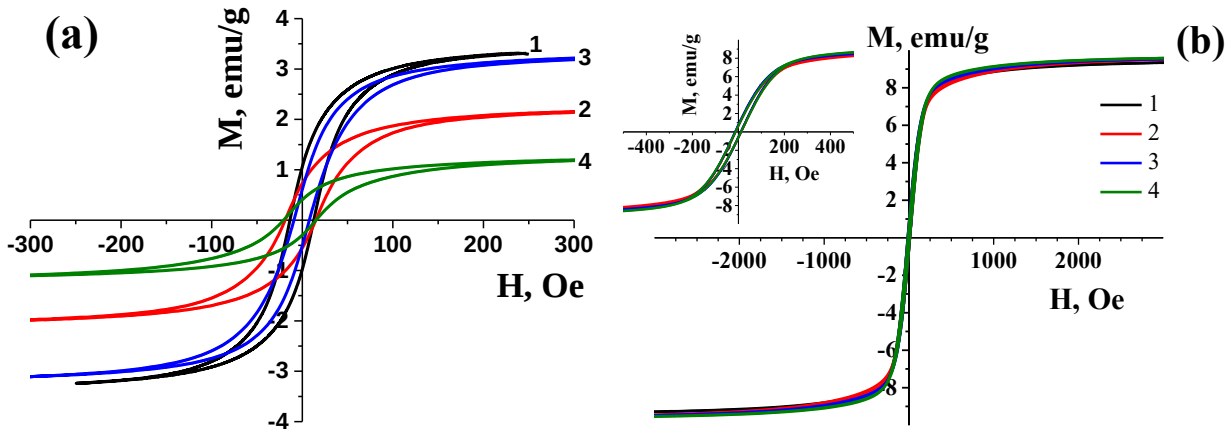

Fig. 5. Hysteresis loops for the ferrite nanoparticles obtained after the heat treatment at 800 °C (a) and ceramic samples after the sintering at 1350 °C (b).

The saturation magnetization of Al-substituted YIG is $M_s = M_s^{YIG}(1-x+2y)$, where M_s^{YIG} = 5 μ_B per formula unit [44]. It implies that for the case where x = 1, the resulting magnetization can only be non-zero when some amount of Al ions is located in octahedral sites.

As seen from Table 3, the maximal value of the saturation magnetization achieved in the nanoparticles under investigation is 3.42 emu/g, which is equivalent to 0.42 μ_B per formula unit. This means that around 4 % of Al ions are located in octahedral sites.

It is noteworthy that a close value of the saturation magnetization (4.1 emu/g) was reported in Ref. [27] for the $Y_3AlFe_4O_{12}$ nanopowders prepared via autocombustion sol-gel technique.

Ceramic samples were synthesized based on the obtained ferrite nanoparticles and their magnetic properties were investigated. It should be noted that the saturation magnetization for all ceramic samples of ferrites after the sintering in the temperature range of 1350-1400 °C (Fig. 5b) is almost the same and it does not depend on the method of synthesis, in contrast to the picture observed on nanoparticles treated at 800 °C.

Table 3. Magnetic parameters of the ferrites

Parameter	*Sample 1*	*Sample 2*	*Sample 3*	*Sample 4*
Parameters of the ferrite nanoparticles obtained after 800 °C				
M_s (emu/g)	3.42	1.765	3.4	1.31
H_c (Oe)	8.435	12.55	8.535	17.935
Parameters of the ceramic samples obtained after heat treatment at 1350°C				
M_s (emu/g)	9.46	9.64	9.67	9.70
H_c (Oe)	12.675	12.76	13.011	12.648

As it was established according to the data of X-ray diffraction and optical microscopy (Fig. 6, 7), all synthesized ceramic samples are single-phase and are visually characterized by the low porosity, in agreement with the calculated values of the density of the synthesized samples (Table 4). At the same time, it should be noted that a reduced porosity of Samples 1 and 2 can be partially caused by the high chemical activity of the nanopowders and presence of the traces of α-Fe_2O_3 (see inset in Fig. 3). At the same time, the presence of α-Fe_2O_3 impurity is not observed in the XRD patterns of the ceramic samples shown in Fig. 6. The average size of the grains in the ceramics (*Samples 1-4*) was approx. 10 μm (Fig. 6) [45].

The results of the investigations of the dielectric constant and the width of the ferromagnetic resonance (FMR) line are listed in Table 4. It follows from the literature sources that dielectric constant of the Al-substituted yttrium-iron garnets equals, as a rule, approx. 15 [13, 46]. Our investigations showed that the value of ε′ lies the range of 13.6-15.4, depending on the method of synthesis. Since for the resonant cavity measurements [37, 38] the error of the measurements can reach 10 %, one can conclude that our data are in a reasonably good agreement with the literature data [47].

Table 4. Physical parameters of the ceramic YIAG garnet ferrites

Parameter	*a*, Å	*V*, Å^3	R_f*	R_{Bragg}**	ρ_{XRD} (g/cm^3)	ρ (g/cm^3)	Porosity (%)	ε'	ΔH (Oe)
Sample 1	12.318(1)	1869.1(3)	7.7	6.3	5.04	4.93	97.8	13.6	46
Sample 2	12.281(4)	1852.6(1)	5.2	8.4	5.08	4.97	97.8	15.4	44
Sample 3	12.321(5)	1870.8(4)	7.2	6.8	5.03	4.96	98.6	14.6	43
Sample 4	12.318(8)	1869.2(2)	6.7	7.1	5.04	4.85	96.2	15.4	35

*R_f is compliance form factor; **R_{Bragg} is Bragg factor

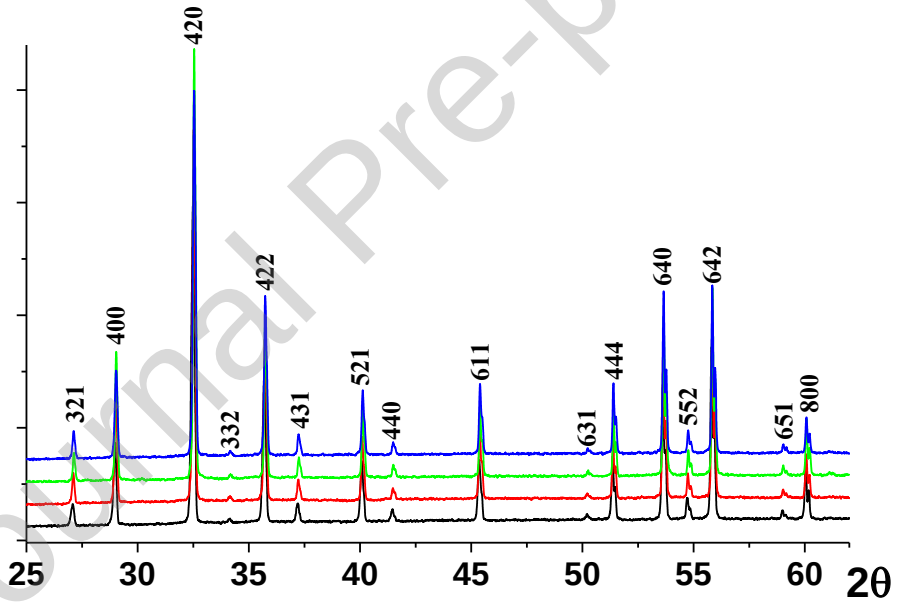

Fig. 6. XRD patterns of the ceramic samples of the ferrites obtained at sintering 1350 °C -1400 °C for 2 h. 1 – *Sample 1*; 2 – *Sample 2*; 3 – *Sample 3*; 4 – *Sample 4*.

The FMR linewidths (~35-45 Oe) are in good agreement with the values reported in literature [13, 47, [48]]. It can be seen that the lowest values of the FMR linewidth demonstrates the sample based on the nanoparticles synthesized by the consecutive precipitation with ammonium solution (*Sample 4*).

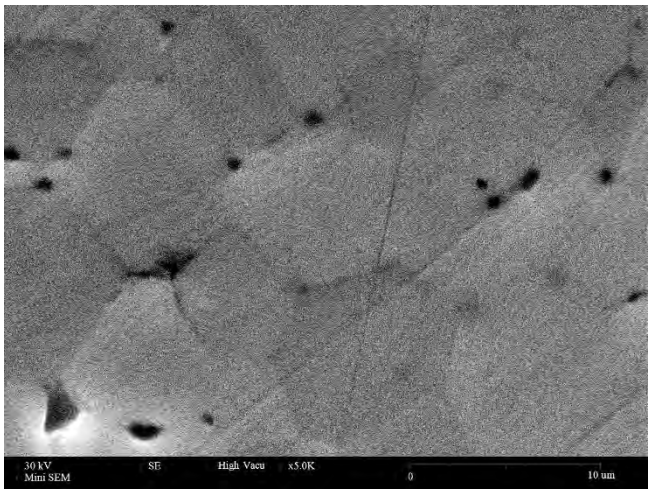

Sample 1

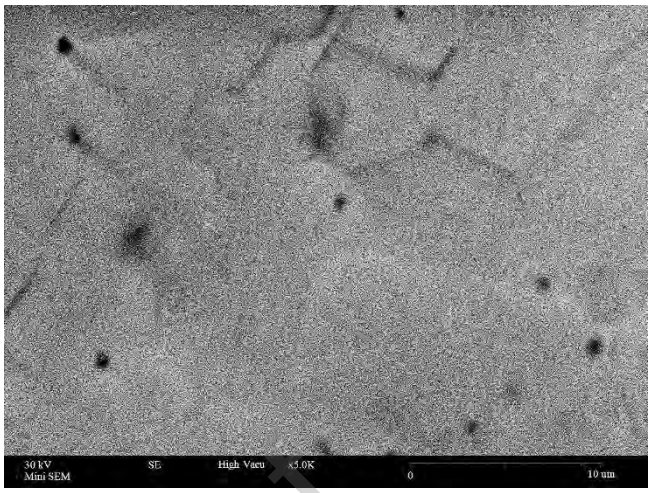

Sample 2

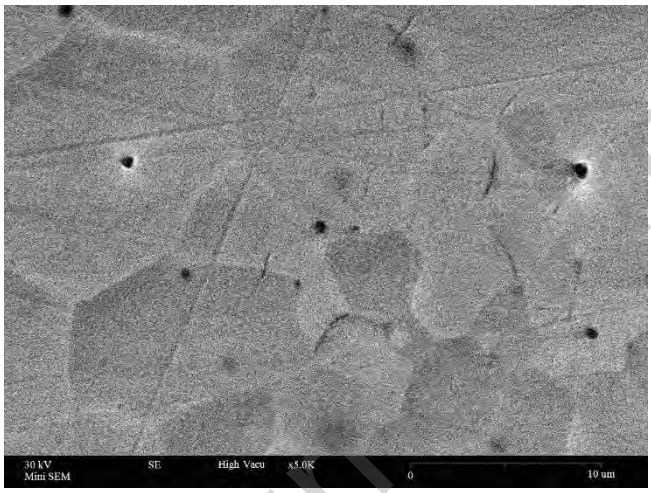

Sample 3

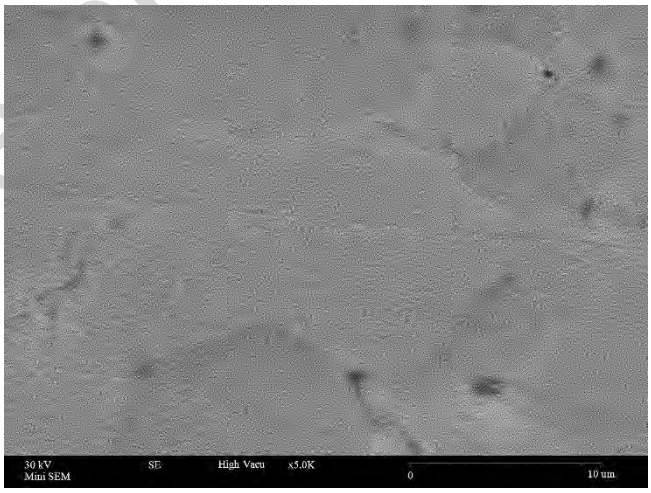

Sample 4

Fig. 7. Micrographs of the polished surfaces of the ceramic samples based on the YIAG ferrite nanoparticles.

Slightly higher ΔH values for the ceramic materials based on *Samples 1 – 3* may originate from the presence of some amount of the sodium ions [49]. One can see that when going from *Sample 1* to *Sample 3,* the FMR linewidth decreases, while the filtration coefficient increases. It is likely that the growth of the filtration coefficient leads to the reduction of the concentration of the sodium ions and this results in the decreasing of the width of the FMR lines. It should be noted,

however, that the values of coercivity and FMR linewidth, obtained in our work, prevail over the typical data reported for the samples synthesized by other methods [46, [50], [51]].

Conclusions

Synthesis of ferrite $Y_3AlFe_4O_{12}$ nanoparticles with the garnet structure was performed by the precipitation in the aqueous solutions at the constant pH during the precipitation of the metal hydroxides. Precipitates were established to have the different filtration coefficient dependently on the precipitation route. The highest filtration coefficient were shown to be observed when at the first stage $Fe(OH)_3$ and $Al(OH)_3$ were precipitated at pH 4 ÷ 4.5 and further $Y(OH)_3$ – at pH 8.8 ÷ 8.9 (*Sample 3*). Crystalline garnet structure of the nanoparticles was established to be formed in one stage after the heat treatment at 800 °C; the average size of the particles was of 50-70 nm. Particles obtained at the lower temperatures were in the amorphous state.

It was shown that the crystalline garnet structure formed faster in the cases of the simultaneous precipitation of the metal hydroxides by NaOH solution at the constant pH (*Sample 1*) or for the case of the first simultaneous precipitation of the mixture of $Fe(OH)_3$ and $Al(OH)_3$ at pH 4 ÷ 4.5 (ions of iron and aluminum are in the same crystallographic sub-lattice) and further precipitation of $Y(OH)_3$ at pH 8.8 ÷ 8.9 (*Sample 3*) than in the cases of *Samples 2* and *4*. Ceramic samples of $Y_3AlFe_4O_{12}$ ferrites with the garnet structure were established to be sintered at the relatively low temperature 1350-1400 °C. Such samples were characterized by the high density and good electrophysical properties.

CRediT authorship contribution statement

Anatolii Belous: Project administration, Conceptualization.

Alexandr Tovstolytkin: Supervision, Project administration.

Oleksandr Fedorchuk: Formal analysis, Investigation.

Yulia Shlapa: Writing - Original Draft.

Serhii Solopan: Investigation, Resources, Methodology, Writing - Original Draft, Visualization.

Borys Khomenko: Investigation, Resources.

Declaration of interests

☒ The authors declare that they have no known competing financial interests or personal relationships that could have appeared to influence the work reported in this paper.

☐The authors declare the following financial interests/personal relationships which may be considered as potential competing interests:

Acknowledgments

The authors are thankful to A.V. Bodnaruk for assistance with magnetic measurements. The work is partially supported by the National Academy of Sciences of Ukraine (Projs. No. 0120U102727 and 0119U100469).

References

[1] Chang, Houchen, et al. "Nanometer-thick yttrium iron garnet films with extremely low damping." *IEEE Magnetics Letters* 5 (2014): 1-4.

[2] Inoue, Mitsuteru, and Toshitaka Fujii. "A theoretical analysis of magneto-optical Faraday effect of YIG films with random multilayer structures." *Journal of applied physics* 81.8 (1997): 5659-5661.

[3] Cheng, Zhongjun, et al. "Saturation magnetic properties of $Y_{3-x}Re_xFe_5O_{12}$ (Re: Gd, Dy, Nd, Sm and La) nanoparticles grown by a sol–gel method." *Journal of Materials Science: Materials in Electronics* 19.5 (2008): 442-447.

[4] Wu, Y. J., et al. "Influence of surfactants on co-precipitation synthesis of Bi-YIG particles." *Journal of alloys and compounds* 470.1-2 (2009): 497-501.

[5] Sánchez, Rodolfo Daniel, et al. "Particle size effects on magnetic properties of yttrium iron garnets prepared by a sol–gel method." *Journal of magnetism and magnetic materials* 247.1 (2002): 92-98.

[6] Garskaite, E., et al. "On the synthesis and characterization of iron-containing garnets ($Y_3Fe_5O_{12}$, YIG and $Fe_3Al_5O_{12}$, IAG)." *Chemical physics* 323.2-3 (2006): 204-210.

[7] Chen, Y. F., et al. "The influence of Fe concentration on $Y_3Al_{5-x}Fe_xO_{12}$ garnets." *Microelectronic engineering* 81.2-4 (2005): 329-335.

[8] Serga, A. A., A. V. Chumak, and B. Hillebrands. "YIG magnonics." *Journal of Physics D: Applied Physics* 43.26 (2010): 264002.

[9] Kamada, O., H. Minemoto, and S. Ishizuka. "Mixed rare-earth iron garnet (TbY) IG for magnetic field sensors." *Journal of Applied Physics* 61.8 (1987): 3268-3270.

[10] Li, Haiyan, and Yuheng Guo. "High microwave absorption characteristic nanomaterial preparation and mechanism analysis." *Journal of Alloys and Compounds* 765 (2018): 936-942.

[11] Kirihara, Akihiro, et al. "Spin-current-driven thermoelectric coating." *Nature materials* 11.8 (2012): 686-689.

[12] Li, Wei, et al. "Ferrite-based metamaterial microwave absorber with absorption frequency magnetically tunable in a wide range." *Materials & Design* 110 (2016): 27-34.

[13] Sharma, Vinay, and Bijoy Kumar Kuanr. "Magnetic and crystallographic properties of rare-earth substituted yttrium-iron garnet." *Journal of Alloys and Compounds* 748 (2018): 591-600.

[14] Mezin, N. I., N. Yu Starostyuk, and S. V. Yampolskii. "Growth and properties of yttrium-iron garnet films with a higher iron content." *Journal of Magnetism and Magnetic Materials* 442 (2017): 189-195.

[15] Baños-López, E., et al. "Crystal structure and magnetic properties of cerium-doped YIG: Effect of doping concentration and annealing temperature." *Journal of Alloys and Compounds* 730 (2018): 127-134.

[16] Akhtar, Majid Niaz, et al. "Structural and electromagnetic evaluations of YIG rare earth doped (Gd, Pr, Ho, Yb) nanoferrites for high frequency applications." *Ceramics International* 43.18 (2017): 17032-17040.

[17] Golkari, M., H. Shokrollahi, and H. Yang. "The influence of Eu cations on improving the magnetic properties and promoting the Ce solubility in the Eu, Ce-substituted garnet synthesized by the solid state route." *Ceramics International* 46.7 (2020): 8553-8560.

[18] Basavad, M., et al. "Structural, magnetic and magneto-optical properties of the bulk and thin film synthesized cerium-and praseodymium-doped yttrium iron garnet." *Ceramics International* 46 (2020): 12015–12022.

[19] Li, Haiyan. "Investigation of the structural, magnetic, impedance properties in samarium-doped yttrium iron garnet." *Ceramics International* 46 (2020): 15408–15416.

[20] Akhtar, Majid Niaz, et al. "Structural, magnetic, dielectric and high frequency response of synthesized rare earth doped bismuth nano garnets (BIG)." *Results in Physics* 10 (2018): 784-793.

[21] Peña-Garcia, R., et al. "The extended Bloch's law in yttrium iron garnet doped with Zn, Ni and Co." *Physica E: Low-dimensional Systems and Nanostructures* 103 (2018): 354-360.

[22] Peña-Garcia, R., et al. "Structural and magnetic properties of Ni-doped yttrium iron garnet nanopowders." *Journal of Magnetism and Magnetic Materials* 492 (2019): 165650.

[23] Enayati, Ehsan, Saeedeh Hashemian, and Mohsen Hakimi. "Effect of Bi and Mn doping on the structure and magnetic properties of $Y_3Fe_5O_{12}$ nanopowders synthesized by mechanochemical milling." *Materials Chemistry and Physics* 242 (2020): 122042.

[24] Yang, Yan, et al. "Thermomagnetization characteristics and ferromagnetic resonance linewidth broadening mechanism for Ca-Sn Co-substituted YIG ferrites." *Ceramics International* 44.10 (2018): 11718-11723.

[25] Bhalekar, A. R., and L. N. Singh. "Structural, magnetic and ESR studies of $Y_3Al_xFe_{5-x}O_{12}$ ($0.0 \leq x \leq 1.2$) nanoparticles synthesized by a sol-gel method." *Physica B: Condensed Matter* 570 (2019): 82-93.

[26] Anupama, A. V., et al. "Synthesis of coral-shaped yttrium-aluminium-iron garnets by solution-combustion method." *Ceramics International* 44.3 (2018): 3024-3031.

[27] Musa, Makiyyu Abdullahi, et al. "Structural and magnetic properties of yttrium iron garnet (YIG) and yttrium aluminum iron garnet (YAlG) nanoferrite via sol-gel synthesis." *Results in physics* 7 (2017): 1135-1142.

[28] Akhtar, Majid Niaz, et al. "Structural and magnetic properties of yttrium iron garnet (YIG) and yttrium aluminum iron garnet (YAIG) nanoferrites prepared by microemulsion method." *Journal of Magnetism and Magnetic Materials* 401 (2016): 425-431.

[29] Zeng, Min. "CO-precipitation synthesis of iron-containing garnets $Y_3Al_{5-x}Fe_xO_{12}$ and their magnetic properties." *Journal of Magnetism and Magnetic Materials* 393 (2015): 370-375.

[30] Sharma, Vinay, et al. "Synthesis and characterization of yttrium iron garnet (YIG) nanoparticles-Microwave material." *AIP Advances* 7.5 (2017): 056405 .

[31] Komarneni, Sridhar, et al. "Microwave-hydrothermal synthesis of nanophase ferrites." *Journal of the American Ceramic Society* 81.11 (1998): 3041-3043.

[32] Akhtar, Majid Niaz, et al. "$Y_3Fe_5O_{12}$ nanoparticulate garnet ferrites: Comprehensive study on the synthesis and characterization fabricated by various routes." *Journal of Magnetism and Magnetic Materials* 368 (2014): 393-400.

[33] Sadhana, K., S. Ramana Murthy, and K. Praveena. "Structural and magnetic properties of Dy^{3+} doped $Y_3Fe_5O_{12}$ for microwave devices." *Materials Science in Semiconductor Processing* 34 (2015): 305-311.

[34] Schwertmann, U. T., and W. R. Fischer. "Natural “amorphous” ferric hydroxide." *Geoderma* 10.3 (1973): 237-247.

[35] Whitaker, Stephen. "Flow in porous media I: A theoretical derivation of Darcy's law." *Transport in porous media* 1.1 (1986): 3-25.

[36] Barbieri, Luisa, et al. "Crystallization of (Na_2O–MgO)–CaO–Al_2O_3–SiO_2 glassy systems formulated from waste products." *Journal of the American Ceramic Society* 83.10 (2000): 2515-2520.

[37] Basics of Measuring the Dielectric Properties of Materials. Retrieved from https://www.keysight.com/zz/en/assets/7018-01284/application-notes/5989-2589.pdf

[38] Agilent Technologies. Basics of Measuring the Dielectric Properties of Materials. http://academy.cba.mit.edu/classes/input_devices/meas.pdf.

[39] Popov, M. A., et al. "Microwave composite structures on the base of nickel-zinc ferrite $Ni_{1-x}Zn_xFe_2O_4$ nanoparticles in the photopolymer matrix." *Journal of Magnetism and Magnetic Materials* 469 (2019): 398-404.

[40] Gräper, W. "B. Susceptibility data at low temperatures in the vicinity of an ordering temperature." *Part B.* Springer, Berlin, Heidelberg, 1970. 4-6.

41 Casey, William H. "Large aqueous aluminum hydroxide molecules." *Chemical reviews* 106.1 (2006): 1-16.

42 Lodding, William, and Laurence Hammell. "Differential thermal analysis of hydroxides in reducing atmosphere." *Analytical Chemistry* 32.6 (1960): 657-662.

43 Motlagh, Z. Azadi, M. Mozaffari, and J. Amighian. "Preparation of nano-sized Al-substituted yttrium iron garnets by the mechanochemical method and investigation of their magnetic properties." *Journal of Magnetism and Magnetic Materials* 321.13 (2009): 1980-1984.

44 Thongmee, S., P. Winotai, and I. M. Tang. "Local field fluctuations in the substituted aluminum iron garnets, $Y_3Fe_{5-x}Al_xO_{12}$." *Solid State Communications* 109.7 (1999): 471-476.

45 Ali, Wan Fahmin Faiz Wan, et al. "Sintering and grain growth control of high dense YIG." *Ceramics International* 42.12 (2016): 13996-14005.

46 Borsari, E., et al. "Microwave-hydrothermal synthesis of $Y_3Fe_{3.35}Al_{1.65}O_{12}$ nanoparticles for magneto-hyperthermia application." *Journal of Materials Science: Materials in Electronics* 29.21 (2018): 18020-18029.

47 https://ferrite-domen.com/images/pr8/microwave_ferrites_2018_en.pdf

48 Mahender, C., et al. "Low-loss YIG thick films for microwave applications." *Ceramics International* 45.4 (2019): 4316-4321.

49 Ramesh, M., et al. "Effect of sodium doping of rare-earth iron garnet films on magnetic and magneto-optic properties." *Journal of applied physics* 70.10 (1991): 6289-6291.

50 Li, Haiyan, and Yuheng Guo. "Synthesis and characterization of YIG nanoparticles by low temperature sintering." *Journal of Materials Science: Materials in Electronics* 29.11 (2018): 9369-9374.

51 Ramesh, T., et al. "Microwave-hydrothermal synthesis of $Y_3Fe_5O_{12}$ nanoparticles: sintering temperature effect on structural, magnetic and dielectric properties." *Journal of Superconductivity and Novel Magnetism* 31.6 (2018): 1899-1908.

Graphical abstract

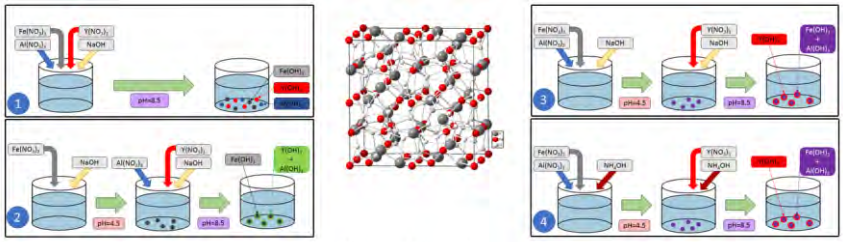

Parameters of the ceramic ferrite samples

Parameter	Sample 1	Sample 2	Sample 3	Sample 4
ρ (g/cm³)	4.93	4.97	4.96	4.85
ε'	13.6	15.4	14.6	15.4
ΔH (Oe)	46	44	43	35

Highlights

- $Y_3AlFe_4O_{12}$ nanoparticles have been synthesized by the precipitation in solutions
- Effect of synthesis route of $Y_3AlFe_4O_{12}$ on filtration coefficient has been shown
- Ceramic samples of $Y_3AlFe_4O_{12}$ ferrites have been synthesized at the low temperature
- $Y_3AlFe_4O_{12}$ ceramics has possessed the high density and electrophysical properties